Published in final edited form as:
Phys Med Biol. 2012 May 7; 57(9): 2653–2666. doi:10.1088/0031-9155/57/9/2653.

Hyperthermically induced changes in high spectral and spatial resolution MR images of tumor tissue – a pilot study

Sean Foxley[1], **Xiaobing Fan**[1], **Jonathan River**[1], **Marta Zamora**[1], **Erica Markiewicz**[1], **Shunmugavelu Sokka**[2], and **Gregory S Karczmar**[1,*]

[1]Department of Radiology, University of Chicago, Chicago, IL, 60637

[2]Philips Healthcare, Andover, MA, 01810

Abstract

This pilot study investigated the feasibility of using MRI based on BOLD (blood oxygen level dependent) contrast to detect physiological effects of locally induced hyperthermia in a rodent tumor model. Nude mice bearing AT6.1 rodent prostate tumors inoculated in the hind leg were imaged at 9.4T scanner using a multi-gradient echo pulse sequence to acquire high spectral and spatial resolution (HiSS) data. Approximately 6 °C increases were produced locally in tumor tissue using fiber optic guided light from a 250 W halogen lamp. HiSS data were acquired over three slices through the tumor and leg both prior to and during heating. Water spectra were produced from these datasets for each voxel at each time point. Time dependent changes in water resonance peak width were measured during 15 minutes of localized tumor heating. The results demonstrated that hyperthermia produced both significant increases and decreases in water resonance peak width. Average decreases in peak width were significantly larger in the tumor rim than in normal muscle ($p = 0.04$). The effect of hyperthermia in tumor was spatially heterogeneous, i.e., the standard deviation of the change in peak width was significantly larger in the tumor rim than in normal muscle ($p = 0.005$). Therefore, mild hyperthermia produces spatially heterogeneous changes in water peak width in both tumor and muscle. This may reflect heterogeneous effects of hyperthermia on local oxygenation. The peak width changes in tumor and muscle were significantly different, perhaps due to abnormal tumor vasculature and metabolism. Response to hyperthermia measured by MRI may be useful for identifying and/or characterizing suspicious lesions as well as guiding development of new hyperthermia protocols.

Keywords

Hyperthermia; MRI; spectroscopic imaging; cancer

1. Introduction

The purpose of this pilot study was to determine whether magnetic resonance imaging (MRI) is sensitive to the physiological effects of mild hyperthermia, serving as an initial step towards use of MRI to guide development and clinical applications of hyperthermia. Locally induced hyperthermia (Chichel *et al* 2007), typically identified as an increase in tissue temperature to 40-48 °C, is generally used clinically to treat small, often superficial tumors. Such an elevation in tumor tissue temperature, in conjunction with varying durations of exposure, increases sensitivity to other treatment modalities (van der Zee 2002). Further, at

[*]**Address correspondence to:** University of Chicago Department of Radiology – MC2026 5841 S. Maryland Ave. Chicago, Illinois 60637 Phone: (773) 702-0214 FAX: (773) 702-1161 gskarczm@uchicago.edu.

higher temperatures and/or exposure durations (i.e. increased thermal dose), hyperthermia alone will produce cancer cell death (Hildebrandt *et al* 2002).

Micro-electrode measurements demonstrate that both temperature changes and the consequent physiological responses (e.g. changes in blood oxygenation concentration) are heterogeneously distributed within the tumor (Kelleher *et al* 1995). This suggests the need to more completely characterize the response to hyperthermia at high spatial resolution across the whole tumor and surrounding tissue. Such measurements could be used clinically to optimize therapy for individual patients, and pre-clinically to guide development of new approaches to thermal therapy. In addition, since the response of tumor tissue to hyperthermia is likely to be different from that of normal tissue (reflecting the physiologic properties of tumors), the use of imaging methods to non-invasively detect the response to a 'temperature challenge' could have diagnostic utility. Single point and multifocal measurement techniques, such as the use of needle probes, provide useful information regarding local tissue response to hyperthermia (e.g. changes in oxygen partial pressure (pO_2)) (Kelleher *et al* 2010, Song *et al* 2001), but these measurements are invasive and cannot routinely provide high resolution images of this response across a significant volume of tissue.

MRI allows measurement of temperature changes in tumors based on proton resonance frequency (Rieke *et al* 2008), and is frequently used to measure the hyperthermic response of tumor tissue. Moreover, MRI may be sensitive to physiological changes caused by hyperthermia. In particular changes in local oxygen concentration are of great interest because of their effect on radiation therapy. A number of MRI methods are sensitive to BOLD (blood oxygen level dependent) contrast associated with tumor vasculature, due to the effect ofparamagnetic deoxygemoglobin on water resonance T_2^* (R_2^*) as well as proton resonance frequency (Al-Hallaq *et al* 2002, Chu *et al* 1990, Haacke *et al* 2004, Karczmar *et al* 1994, Ogawa *et al* 1990, Reichenbach *et al* 1997). In fact, changes in proton resonance frequency due to changes in local oxygenation may cause errors in temperature measurements based on proton resonance frequency, and conversely, local temperature gradients caused by hyperthermia can affect water resonance linewidth and BOLD contrast. MRI methods are not as specific and quantitative as direct micro-electrode measurements since changes in T^*_2 and resonance frequency can be caused by other processes not related to blood oxygenation. However, MRI methods are generally non-invasive and, in particular, BOLD measurement techniques potentially allow repeated measurements of physiological responses to hyperthermia at high spatial resolution.

In this research, a novel method was developed to induce local hyperthermia in a rodent cancer model during MRI scans. Fiber optic guided light produced from a 250 W halogen light source was used to increase local temperature by 5 - 6 °C in small rodent tumors and surrounding normal tissue. Physiologic changes during hyperthermia were detected by using high spectral and spatial resolution (HiSS) MRI (Guilfoyle *et al* 1985, Mansfield 1984, Webb *et al* 1989). HiSS imaging was used because it allowed accurate measurements of the water resonance frequency and peak width (the full width in Hz at half the maximum signal intensity of the resonance). Changes in resonance frequency and peak width are likely to be affected by both temperature and blood oxygenation, respectively (Du *et al* 2005, Foxley *et al* 2009, Oikawa *et al* 1997). Proton resonance frequency and T^*_2 (R^*_2) can be measured in the time domain using multi-gradient echo imaging as long as the water signal can be well-approximated by a simple mono-exponential or bi-exponential decay (Robinson *et al* 2003). However, the water resonance from small voxels *in vivo* may be contaminated by signals from fat and may have a complicated non-Lorentzian lineshape (Al-Hallaq *et al* 2002) due to the highly heterogeneous micro-environment. Therefore, resonance frequency, peak width,

and spectral lineshape are most accurately and conveniently evaluated in the spectral domain (Oikawa *et al* 1997).

2. Materials and Methods

2.1. Tumor model

Ten experiments (2 bench experiments and 8 hyperthermia experiments) were performed using 10 different male nude mice bearing AT6.1 rodent prostate tumors inoculated in the hind leg. Tumor volumes were 0.25 ± 0.05 cm^3 (approximated to be ellipsoids with volume $4/3\pi abc$). All procedures performed on animals followed protocols approved by the Institutional Animal Care and Use Committee and were in compliance with the Animal Welfare Act and the NIH Guide for the Care and Use of Laboratory Animals. Mice were immobilized on a Plexiglas board with vet wrap and tape and anesthetized with 1.5-2% isoflurane gas mixed with medical air (2 L/min) delivered through a mask. Temperature, ECG, and respiration rate were continuously monitored throughout each experiment (SA Instruments, Stony Brook, NY). Temperature was maintained using a warm air blower fed into the bore of the magnet.

2.2. Hyperthermia induction

Local hyperthermia was induced during MRI experiments in the tumor bearing mouse leg using light from a 250 W halogen bulb (figure 1). A 1 m long, 1 cm diameter quartz rod was fixed to the light source and used as a light pipe (figure 1(a)). A 1.5 m length of 3 mm diameter fiber optic cable was used, where one end of the cable was manufactured with a 1 cm length of cable following a 90° bend. The straight end of the fiber optic cable was attached to the distal end of the quartz rod from the light source (figure 1(b)), and the bent end of fiber optic cable was taped flush to the side of the mouse leg. This was done in such a way that the cross-section of cable face was bisected by the tumor/normal muscle interface (figure 1(c)). This insured that a small region of both normal muscle and tumor tissue had similar exposure to penetrating light. The fiber optic cable produced very modest magnetic susceptibility artifacts that affected HiSS images in pixels within ~1 mm of the tip of the cable.

Light from a tungsten-halogen lamp produces a broadband wavelength output of photons that is approximated by a Poisson distribution, with a peak radiant flux at ~900 nm (within the near infrared (NIR)) and extending well in to the longer wavelength infrared-B spectrum (1400-3000 nm). Tissue has a characteristic NIR ‘window’ (~700-900 nm) where photon scatter is the dominant tissue/photon interaction and photons achieve a maximum depth of penetration, often resulting in complete transmission through thinner tissue samples. At wavelengths above and below this window, photons from the tungsten-halogen source are increasingly absorbed at shallow depths, producing the observed changes in temperature in the rodent leg and tumor.

2.3. Bench experiments

Bench experiments (n = 2) were performed as gold standard measurements of the temperature changes produced by the light. Measurements were taken with two temperature needle probes; one was placed subcutaneously at the tumor surface, the other ~1.5 mm into the tumor tissue. The mouse setups for bench and subsequent MRI experiments were identical. Temperature was measured every 2 minutes and 30 seconds for 6 time points (a total of 15 minutes) with the light turned off and 6 more time points with the light on.

These time series data, including the average baseline and the 6 time points during hyperthermia, were fit with the equation:

$$s(t) = A\left(1 - e^{-\alpha \cdot t}\right) \quad (1)$$

where, 'A' represents the temperature plateau, or maximum change in temperature due to heating, and α is the rate of temperature change. This equation was used because the time dependent change in temperature in each voxel, *s(t)*, due to a constant heat source, exponentially approaches a maximum steady state value (A), assuming a fairly homogeneous tissue and homogeneous blood flow (Nitzan *et al* 1985). Data were confounded by limited signal-to-noise ratio, therefore this simple model proved adequate to fit the data acquired.

2.4. MRI data collection protocol

MR signal was detected with a small home-built low-pass birdcage coil designed for rodent imaging. Mice were imaged using a 9.4 T Bruker BioSpec 33 cm horizontal bore scanner (Billerica, MA) with 11.6 cm inner diameter, actively shielded gradient coils (maximum constant gradient strength for all axes: 230 mT/m). Tumor localization was performed using a multi-slice gradient echo acquisition (pulse sequence = fast low angle shot, repetition time (TR)/echo time (TE) = 300/4.1 ms, array size = 128 × 128, field of view (FOV) = 25.6 mm, slice thickness = 1.0 mm, number of excitations (NEX) = 2) and a high resolution fast spin echo acquisition (pulse sequence = rapid acquisition with refocused echoes (RARE), TR = 4000 ms, RARE factor = 4, effective TE = 22.8 ms, array size = 256 × 256, FOV = 25.6 mm, slice thickness = 1.0 mm, NEX = 2). 'Fastmap' (Gruetter 1993) was performed on an isotropic voxel sized to encompass both the tumor and the proximal normal muscle to improve localized shimming to the second order. This iterative technique produces estimates of B_0 along orthogonal directions within the defined voxel, then approximates the first and second order gradient strengths required to reduce macroscopic B_0 gradients.

Three slices were selected from localization scans for subsequent HiSS imaging. HiSS data were acquired using a multi-gradient echo (MGE) pulse sequence with the same spatial resolution and slice thickness as the aforementioned gradient echo images (first echo TE = 2.0 ms, subsequent echo spacing = 2.4 ms, number of echoes = 64, 2D spatial array size = 128 × 128, receiver bandwidth = 101.01 kHz, nominal spectral resolution = 6.5 Hz, flip angle = 90°, NEX = 2). HiSS imaging was respiratory-gated to minimize motion artifacts associated with breathing. Because of this, the TR was determined by the respiration rate (typically ~1200 ms) and produced scan lengths approximately equal to the temperature measurement sampling rate previously mentioned. Anesthesia levels were continuously monitored to maintain a constant respiration rate.

Hyperthermia MRI experiments (n = 8) were performed with 6 HiSS datasets acquired at normal temperature and 6 with the light source turned on. Mouse core body temperature was constantly monitored and at no point during heating did the core temperature of the mouse change by more than ±0.1 °C.

2.5. HiSS data processing

Data were processed and analyzed using IDL (ITT, White Plains, NY). The MGE pulse sequence includes an excitation pulse followed by an oscillating readout gradient train; this allows for a voxel-byvoxel sampling of the free induction decay. Each slice of complex raw HiSS data was initially reformatted into a three dimensional array ($k_x \times k_y \times$ time). 3D arrays were Fourier transformed in all three dimensions to produce two spatial and one spectral dimension ($x \times y \times \nu$). Spectral ghosting was removed by correcting the error in phase between the even and odd echoes (Du *et al* 2003) of the gradient echo train. Estimates of the frequency of the water peak were obtained with a frequency shifting method (Fan *et al*

2002); as a result, the effective spectral resolution was higher than the nominal resolution of 6.5 Hz. The baseline for each spectrum was determined and subtracted (Al-Hallaq *et al* 2002); and water resonance peak widths (full-width at half max) were calculated. Fat content in the rodent hind leg was low and, therefore, did not interfere with peak width computations.

For each slice imaged in each experiment, 'tumor,' 'tumor rim,' 'tumor center,' and 'normal muscle' regions of interest (ROIs) were manually segmented from spin echo images; these ROIs were used for all subsequent analyses. After the tumor-muscle interface (outer border of the 'rim') was manually traced on the T_2-weighted image, the tumor rim ROI was defined as the 10 pixel thick band towards the center of the tumor from this interface. The tumor center ROI was defined as everything 10 pixels further towards the tumor center from the inner border of the 'rim'.

2.6. B_0 time series data analyses

A B_0 map was produced from the HiSS dataset at each time point by determining the voxel-by-voxel relative spectral location of the peak of the water resonance (Sarkar *et al* 1999). The B_0 map was used to estimate changes in temperature due to heating (Kuroda 2005, Rieke *et al* 2008). A time series of B_0 subtraction datasets was produced for each experiment according to the following protocol:

- **i.** An average baseline B_0 map was constructed from the 6 baseline B_0 maps.
- **ii.** The average B_0 map was subtracted from all 12 time points in the series to produce a plot of the change in B_0 vs. time for each voxel.

The average change in B_0 over tumor and normal muscle ROIs was calculated from the B_0 difference images. These changes were fit on a voxel-by-voxel basis with equation (1) to identify changes in B_0 that approximately matched the time course of the temperature change measured by the invasive probes. No restrictions were placed on the value of 'α', but for fits of changes in B_0, α values were similar to those obtained from bench experiments (approximately 0.7 min^{-1}). In principle, α can provide valuable information regarding the kinetics of the response to thermal energy; however, α was not evaluated here due to the relatively low temporal resolution of the data.

An 'A' map (A_{Bo}) was produced with units in number of bins (i.e. the number of points in the spectral direction). A_{Bo} maps were converted from bins to °C by multiplying by the spectral resolution of the HiSS dataset (6.5 Hz per bin) and dividing by the temperature dependent water resonance peak shift of −4 Hz per degree at 9.4 Tesla (−0.01 ppm/°C) (Hindman 1966). Thus, A_{Bo} is the maximum change in temperature during heating.

2.7. Peak width (PW) time series data analyses

The water spectrum PW was determined on a voxel-by-voxel basis at each time point. Images of changes in PW were produced following the protocol previously described for B_0 difference datasets. Equation (1) was used to fit the voxel-by-voxel change in water PW as a function of time, and A maps (as previously described) were produced (A_{PW}). A_{PW} is the largest change in water resonance peak width during heating (in Hz). No restrictions were placed on α when fitting the data; however, as with changes in B_0, α for fits of changes in PW were similar to those obtained from bench experiments. This procedure picks out changes in peak width that approximately follow the exponential time course of the temperature changes measured by probes and from water resonance frequency. There may have been changes in peak width that did not follow this exponential time course, but these changes were not evaluated in the present preliminary study.

Time dependent variability in the change in water PW was determined from the control (i.e. baseline) measurements. This variability was used to filter out pixels with excessive drift/variability using the following protocol:

- **i.** The first baseline PW image was subtracted from the last baseline PW image. This difference was considered to be time dependent physiologic noise and/or drift in the water resonance PW. Attempts to model variability and drift over the 6 baseline images for each voxel introduced large errors; therefore this method was selected as a more reliable alternative. Note, however, that this method represents a conservative approach to identifying voxels with excessive drift and variability.
- **ii.** The standard deviation of the water resonance peak width (in Hz) over the normal muscle ROI was computed for the subtraction image produced in step (i).
- **iii.** Pixels in the difference images produced in step (i) with values greater than the standard deviation computed in step (ii) were removed from all subsequent PW analyses; signal from these voxels was considered to be too unstable for further analysis. Approximately 30% of voxels at the tumor rim, and 18% at the tumor center and in muscle were eliminated due to low signal-to-noise ratio and instability.

It is likely that increases and decreases in water resonance peak width reflect decreases and increases in blood oxygenation respectively (Al-Hallaq *et al* 2002, Robinson *et al* 2003). These changes can be very spatially heterogeneous in tumors (Al-Hallaq *et al* 2002, Sun *et al* 2008). Therefore, positive and negative changes in water resonance peak width were measured independently. The average positive and negative A_{PW} values were computed over tumor rim, tumor center, and normal muscle ROIs. A Shapiro-Wilk test demonstrated that the average over 8 positive A_{PW} values and the average over 8 negative A_{PW} values (for each type of ROI) followed a Gaussian distribution. Therefore, ANOVA followed by a Games-Howell post hoc test was used to compare average baseline values of A_{PW} and changes in A_{PW} during hyperthermia.

3. Results

Figure 2 shows plots of time dependent changes during hyperthermia. Figure 2(a) is the change in temperature measured using conventional temperature probes in bench experiments at two positions (tumor surface and 1.5 mm deep in the tumor). The temperature measured by the subcutaneous needle probe (SubQ) was approximately 0.75 °C lower than the temperature measured by the probe placed 1.5 mm deep in the tumor due to more surface cooling. Figure 2(b) is the change in temperature with large standard deviations based on the change in B_0 during MRI experiments, averaged over all experiments for both tumor and normal muscle ROIs. Equation (1) provided excellent fits to the temperature vs. time data obtained from both probes ($R^2 > 0.995$) as well as to the change in average B_0 as a function of time ($R^2 > 0.996$) for both muscle and tumor. The average maximum temperature changes over the whole tumor detected HiSS MRI (figure 2(b)) were slightly higher than, but consistent with, those measured by the probe (figure 2(a)). Temperature maps produced from B_0 maps (e.g. figure 3(b)) did not show the temperature gradient detected by the temperature probes. Differences between MRI thermography and probe measurements may be due to limited spectral resolution of MRI and/or changes in blood oxygenation (or other physiologic changes) that affect local magnetic susceptibility (see discussion of water linewidth changes, below).

Figure 3 shows a typical (a) spin echo image of a tumor bearing hind leg as well as the corresponding (b) A_{Bo} and (c) A_{PW} maps. Red-scale voxels indicate increasingly positive values (dark to light red); blue-scale voxels indicate increasingly negative values (dark to

light blue). The 'blue' area indicating decreased temperature near the tip of the fiber optic cable in figure 3(b) is likely due to modest susceptibility artifacts produced by the probe. The temperature map shows a maximum increase of approximately 6°C during hyperthermia, but does not show a temperature gradient across tumor and muscle. Figure 3(c) shows maximum absolute changes in water peak width (in Hz). Largest negative changes predominantly occur in the tumor rim where dense tumor micro-vasculature is typically located and may indicate large changes in blood oxygenation concentration. The largest changes in peak width (both positive and negative) do not correspond with the areas of largest temperature increase. In this experiment, a shift from positive to negative changes in A_{PW} in muscle occurs at the interface between two muscle bundles, evident in the T_2-weighted image (white arrow).

Figure 4 shows modulus spectra from a single voxel acquired before (1st six) and during hyperthermia (2nd six) in tumor (dark line) and muscle (gray line). These spectra demonstrate the high signal-to-noise ratio of the data, and show changes in water resonance linewidth during hyperthermia. Generally, the maximum amplitude of spectra in tumor was much larger than in muscle.

The average baseline (i.e. pre-hyperthermia) water resonance peak widths in the tumor rim, tumor center, and normal muscle ROIs were 39.8 ± 2.7 Hz, 32.6 ± 6.2 Hz, and 44.5 ± 3.3 Hz, respectively. These values are all significantly different from one another ($p < 0.04$, by ANOVA followed by a Games-Howell post hoc test). The average peak width was narrowest at tumor center and broadest in muscle.

Table 1 reports both the mean (a) positive and (b) negative A_{PW} values, indicating the average voxel-by-voxel change in peak width (Hz) due to hyperthermia (note that a positive A_{PW} value signifies an increase in peak width and a negative A_{PW} value, a decrease). As the table indicates, both the mean positive and negative A_{PW} values were significantly greater (in absolute value) than the variance computed from baseline data from the same ROI ($p < 0.0003$, by a two-tailed, unpaired Student's t-test) for all 3 ROI's. This indicates that there were significant changes (both positive and negative) in the water resonance peak width due to hyperthermia in each ROI. Negative changes in peak width (i.e. mean negative A_{PW}) in tumor rim (−12.9 ± 4.5 Hz) were significantly larger ($p = 0.04$, by analysis of variance (ANOVA) followed by a Games-Howell post hoc test) than in normal muscle (−7.9 ± 1.4 Hz). Positive changes in peak width (i.e. mean positive A_{PW}) were somewhat larger in tumor rim (10.0 ± 3.2 Hz) than in muscle (7.0 ± 2.3 Hz), and this difference was only modestly significant ($p = 0.08$, by ANOVA followed by a least significant difference (LSD) post hoc test). The absolute mean negative A_{PW} over tumor rim was larger than the absolute positive A_{PW} value with modest statistical significance ($p = 0.07$, by a two-tailed, paired Student's t-test) as well. The number of voxels with positive and negative A_{PW} values was approximately equal.

Finally, the mean standard deviation of A_{PW} over all data for each ROI was determined over all experiments as a measure of the spatial heterogeneity of the response to hyperthermia. The mean standard deviation was significantly larger in the tumor rim (26.1 ± 8.2 Hz) than in the tumor center and in normal muscle (14.6 ± 5.7 Hz, $p = 0.001$; and 16.2 ± 4.3 Hz, $p = 0.005$, respectively, by ANOVA followed by a LSD post hoc test).

4. Discussion

The results demonstrate that HiSS MRI detects significant changes in water resonance peak width due to modest (~6 °C) increases in temperature. The physiologic responses were spatially heterogeneous and included both increases and decreases in peak width, suggesting

increased oxygenation in some regions and decreased oxygenation in others. The changes in water resonance peak width were not correlated with temperature changes (figure 3). This suggests that physiologic changes in tumors due to hyperthermia may occur in areas where the temperature change is modest. Previous studies using oxygen-measuring probes demonstrated that mild temperature hyperthermia can increase oxygen tension in tumors (Shakil *et al* 1999, Song *et al* 2001), presumably by dilating tumor blood vessels. More recently Sun *et al* (2008) showed that mild temperature hyperthermia decreased hypoxia in the regions with relatively well-perfused blood vessels, but increased hypoxia in regions that were poorly perfused. These heterogeneous changes are consistent with the negative and positive changes in A_{PW} detected by HiSS. Because the changes were very spatially heterogeneous, positive and negative changes were evaluated independently in the present research. The changes in A_{PW} may be related to local level of deoxyhemoglobin, changes in vasodilation, and/or changes in hematocrit. Further study is required to directly correlate the observed changes in the water resonance with changes in local physiology.

Theoretical and experimental evidence demonstrates that the water resonance is affected by changes in local bulk magnetic susceptibility (Chu *et al* 1990, Karczmar *et al* 1994, Reichenbach *et al* 1997, Spees *et al* 2001, Sukstanskii *et al* 2001, Yablonskiy *et al* 1994) caused by changes in tumor blood oxygenation (Al-Hallaq *et al* 2002, Foxley *et al* 2009). Changes in water resonance peak width were larger in tumor rim than in surrounding muscle. These results are consistent with the findings of Kelleher *et al* (1995), who employed microelectrodes to establish that tumor and normal muscle vasculature respond differently to hyperthermia. This is predominantly due to abnormalities in tumor vasculature (Song *et al* 1984, Waterman *et al* 1987), which result in changes in tumor blood flow, vascular permeability, and blood oxygenation during hyperthermia that are different from those in normal tissue.

Using a single point O_2-sensitive catheter electrode, tumor pO_2 has been demonstrated to increase (up to 40 %) and peak within 10 minutes of induced hyperthermia (approximately 5 °C above normal temperature) in a rodent tumor model (Kelleher *et al* 2010). Multi-focal measurements in a rodent tumor model demonstrated that this response (elevated pO_2) is also spatially heterogeneous (Kelleher *et al* 1995, Kelleher *et al* 2010). While quantitative measurements of microelectrodes are advantageous, even multi-focal methods are limited in their ability to accurately map changes in pO_2. Therefore, the non-invasive MRI measurements demonstrated here have the potential to complement microelectrode studies. Homogeneous changes in tissue blood flow and oxygenation are desirable to make hyperthermia a more effective adjuvant therapy.

The results reported here constitute the first evidence suggesting that MRI detects spatially heterogeneous changes in tumor oxygenation during mild hyperthermia. However, these results are preliminary in nature. While published work suggests that changes in water resonance peak width are related to changes in tumor blood oxygenation (Du *et al* 2005, Foxley *et al* 2009, Oikawa *et al* 1997), there is as yet no direct evidence that the peak width changes reported here due to hyperthermia correlate with changes in oxygenation. This will require a detailed comparison of micro-electrode and MRI data.

Generally, proton resonance frequency (PRF) shift has been detected by using gradient echo pulse sequence, which can measure temperature changes in seconds. In contrast, in the present study, temperature changes were calculated from a B_0 map generated from HiSS data set, which was acquired with temporal resolution of ~2.5 min. While this relatively low temporal resolution limited sensitivity to rapid changes in temperature, and increased errors due to motion, the relatively high frequency resolution increased sensitivity to temperature, as well as other effects of local magnetic susceptibility, e.g. due to changes in oxygenation.

In fact, the large changes in local blood oxygenation suggested by the significant changes in water resonance linewidth could have caused changes in PRF near blood vessels, thereby leading to errors in temperature measurements. This may explain the discrepancies observed in these experiments between MRI thermometry based on PRF and the micro-electrode measurements. If this is the case, this may suggest limitations of MRI thermometry based on PRF measurement. In future work, other approaches to MRI thermometry, based on longitudinal relaxation time (Matsumoto *et al* 1994) or the diffusion coefficient of water (Bleier *et al* 1991, Le Bihan *et al* 1989) will be evaluated to separate oxygenation changes from temperature effects.

The quality of the data presented here was reduced due to drift and random error, and more work will be required to optimize the experimental protocol so that effects of hyperthermia can be detected with greater sensitivity and reliability. In particular, significant drift in the water resonance during the baseline period increased the threshold for significant changes in 'A' and thus reduced sensitivity to changes caused by hyperthermia. Routine quality assurance scans demonstrate that water resonance peak width in phantoms is narrow and very stable ($< 5.0 \pm 1.0$ Hz per voxel). Thus the variability and baseline drift in these experiments was primarily due to physiologic instability and motion, with a modest contribution from instrumental instability. The drift was consistently larger in the tumor than in muscle, possibly reflecting physiologic fluctuations in the tumor tissue. Use of HiSS imaging at high field increases sensitivity to changes in blood oxygenation, but may also decrease stability. Both physiologic and instrumental parameters that contribute to drift, as well as methods to correct for them, will be examined in future work.

An additional source of variability was the positioning of the fiber optic cable on the hind leg. Palpation of the lesion was used to identify the interface between the tumor and the normal muscle, and this was an imprecise method for proper placement of the fiber optic cable. Further, placement of the fiber optic cable over a densely vascularized portion of the tumor could produce different results than placing it over a region of sparse vasculature. In the future, MR or Ultrasound protocols will be developed to improve positioning and reduce variability.

The polychromatic light source used in this study reliably produced mild hyperthermia. However, future work would benefit from use of a monochromatic light source or high intensity focused ultrasound (HIFU). Monochromatic light would have a well characterized interaction with tissue, thereby producing more predictable temperature profiles. HIFU would produce rapid temperature changes in highly localized regions, and allow studies of short term anatomic and physiologic responses to rapid heating. The HIFU focal point could be 'rastered' across the region of interest to image the response to hyperthermia. Further, HIFU would have the added advantage that surface heating associated with shallow photon penetration would be eliminated.

Data analysis identified changes in the water resonance that occurred with a time course modeled by equation (1). Use of this model increases confidence that the changes in water peak width reported here are correlated with hyperthermia, but this approach may miss other components of the response to hyperthermia that do not have a similar time course. For example, slow metabolic changes or gradual changes in blood flow patterns may be missed by the present approach. A larger study with reduced variability and increased signal-to-noise ratio will be required to detect more subtle, delayed responses to hyperthermia that may be clinically significant and/or diagnostically useful.

5. Conclusion

These preliminary results demonstrate statistically significant changes in water peak width produced by mild, transient hyperthermia, probably reflecting changes in blood oxygenation. Changes are larger in tumors than in normal muscle. Effects of hyperthermia on deoxyhemoglobin concentration may have caused errors in temperature measurements based on water proton resonance frequency. Changes detected using HiSS MRI are spatially heterogeneous, consistent with previous reports (Kelleher *et al* 1995), and may reflect heterogeneous changes in tumor blood oxygenation. The results suggest that the response to a mild 'temperature challenge', combined with MRI, could be used as a diagnostic technique to detect and characterize cancers. In addition, imaging could guide the development of improved hyperthermia protocols that produce the desired change in oxygenation across the tumor. However, clinical and research applications of this approach are limited by drift and variability of the data, and more work is required to optimize the experimental protocol.

Acknowledgments

This work was funded by the NIH (5 R33 CA100996-04) as well as by Philips Healthcare. We would also like to thank James Vosicky for his help with animal preparation and monitoring.

References

Al-Hallaq HA, Fan X, Zamora M, River JN, Moulder JE, Karczmar GS. Spectrally inhomogeneous BOLD contrast changes detected in rodent tumors with high spectral and spatial resolution MRI. NMR Biomed. 2002; 15:28–36. [PubMed: 11840550]

Bleier AR, Jolesz FA, Cohen MS, Weisskoff RM, Dalcanton JJ, Higuchi N, Feinberg DA, Rosen BR, McKinstry RC, Hushek SG. Real-time magnetic resonance imaging of laser heat deposition in tissue. Magn. Reson. Med. 1991; 21:132–7. [PubMed: 1943670]

Chichel A, Skowronek J, Kubaszewska M, Kanikowski M. Hyperthermia – description of a method and a review of clinical applications. Rep. Pract. Oncol. Radiother. 2007; 12:267–275.

Chu SC, Xu Y, Balschi JA, Springer CS Jr. Bulk magnetic susceptibility shifts in NMR studies of compartmentalized samples: use of paramagnetic reagents. Magn. Reson. Med. 1990; 13:239–62. [PubMed: 2156125]

Du W, Du YP, Fan X, Zamora MA, Karczmar GS. Reduction of spectral ghost artifacts in high-resolution echo-planar spectroscopic imaging of water and fat resonances. Magn. Reson. Med. 2003; 49:1113–20. [PubMed: 12768590]

Du W, Karczmar GS, Uftring SJ, Du YP. Anatomical and functional brain imaging using high-resolution echo-planar spectroscopic imaging at 1.5 Tesla. NMR Biomed. 2005; 18:235–41. [PubMed: 15759296]

Fan X, Du W, MacEneaney P, Zamora M, Karczmar G. Structure of the water resonance in small voxels in rat brain detected with high spectral and spatial resolution MRI. J. Magn. Reson. Imaging. 2002; 16:547–52. [PubMed: 12412031]

Foxley S, Fan X, Mustafi D, Haney C, Zamora M, Markiewicz E, Medved M, Wood AM, Karczmar GS. Sensitivity to tumor microvasculature without contrast agents in high spectral and spatial resolution MR images. Magn. Reson. Med. 2009; 61:291–8. [PubMed: 19165878]

Gruetter R. Automatic, localized in vivo adjustment of all first- and second-order shim coils. Magn. Reson. Med. 1993; 29:804–11. [PubMed: 8350724]

Guilfoyle DN, Mansfield P. Chemical-shift imaging. Magn. Reson. Med. 1985; 2:479–89. [PubMed: 4094561]

Haacke EM, Xu Y, Cheng YC, Reichenbach JR. Susceptibility weighted imaging (SWI). Magn. Reson. Med. 2004; 52:612–8. [PubMed: 15334582]

Hildebrandt B, Wust P, Ahlers O, Dieing A, Sreenivasa G, Kerner T, Felix R, Riess H. The cellular and molecular basis of hyperthermia. Crit. Rev. Oncol. Hematol. 2002; 43:33–56. [PubMed: 12098606]

Hindman JC. Proton resonance shift of water in the gas and liquid states. J. Chem. Phys. 1966; 44:4582–4592. 44.

Karczmar GS, River JN, Li J, Vijayakumar S, Goldman Z, Lewis MZ. Effects of hyperoxia on T2* and resonance frequency weighted magnetic resonance images of rodent tumours. NMR Biomed. 1994; 7:3–11. [PubMed: 8068523]

Kelleher DK, Engel T, Vaupel PW. Changes in microregional perfusion, oxygenation, ATP and lactate distribution in subcutaneous rat tumours upon water-filtered IR-A hyperthermia. Int. J. Hyperthermia. 1995; 11:241–55. [PubMed: 7790738]

Kelleher DK, Vaupel P. No sustained improvement in tumor oxygenation after localized mild hyperthermia. Adv. Exp. Med. Biol. 2010; 662:393–8. [PubMed: 20204821]

Kuroda K. Non-invasive MR thermography using the water proton chemical shift. Int. J. Hyperthermia. 2005; 21:547–60. [PubMed: 16147439]

Le Bihan D, Delannoy J, Levin RL. Temperature mapping with MR imaging of molecular diffusion: application to hyperthermia. Radiology. 1989; 171:853–7. [PubMed: 2717764]

Mansfield P. Spatial mapping of the chemical shift in NMR. Magn. Reson. Med. 1984; 1:370–86. [PubMed: 6571566]

Matsumoto R, Mulkern RV, Hushek SG, Jolesz FA. Tissue temperature monitoring for thermal interventional therapy: comparison of T1-weighted MR sequences. J. Magn. Reson. Imaging. 1994; 4:65–70. [PubMed: 8148558]

Nitzan M, Anteby SO, Mahler Y. Transient heat clearance method for regional blood flow measurements. Phys. Med. Biol. 1985; 30:557–63. [PubMed: 4011677]

Ogawa S, Lee TM, Nayak AS, Glynn P. Oxygenation-sensitive contrast in magnetic resonance image of rodent brain at high magnetic fields. Magn. Reson. Med. 1990; 14:68–78. [PubMed: 2161986]

Oikawa H, al-Hallaq HA, Lewis MZ, River JN, Kovar DA, Karczmar GS. Spectroscopic imaging of the water resonance with short repetition time to study tumor response to hyperoxia. Magn. Reson. Med. 1997; 38:27–32. [PubMed: 9211376]

Reichenbach JR, Venkatesan R, Schillinger DJ, Kido DK, Haacke EM. Small vessels in the human brain: MR venography with deoxyhemoglobin as an intrinsic contrast agent. Radiology. 1997; 204:272–7. [PubMed: 9205259]

Rieke V, Pauly K Butts. MR thermometry. J. Magn. Reson. Imaging. 2008; 27:376–90. [PubMed: 18219673]

Robinson SP, Rijken PF, Howe FA, McSheehy PM, van der Sanden BP, Heerschap A, Stubbs M, van der Kogel AJ, Griffiths JR. Tumor vascular architecture and function evaluated by non-invasive susceptibility MRI methods and immunohistochemistry. J. Magn. Reson. Imaging. 2003; 17:445–54. [PubMed: 12655584]

Sarkar S, Heberlein K, Metzger GJ, Zhang X, Hu X. Applications of high-resolution echoplanar spectroscopic imaging for structural imaging. J. Magn. Reson. Imaging. 1999; 10:1–7. [PubMed: 10398971]

Shakil A, Osborn JL, Song CW. Changes in oxygenation status and blood flow in a rat tumor model by mild temperature hyperthermia. Int. J. Radiat. Oncol. Biol. Phys. 1999; 43:859–65. [PubMed: 10098442]

Song CW, Lokshina A, Rhee JG, Patten M, Levitt SH. Implication of blood flow in hyperthermic treatment of tumors. IEEE Trans. Biomed. Eng. 1984; 31:9–16. [PubMed: 6724614]

Song CW, Park H, Griffin RJ. Improvement of tumor oxygenation by mild hyperthermia. Radiat. Res. 2001; 155:515–28. [PubMed: 11260653]

Spees WM, Yablonskiy DA, Oswood MC, Ackerman JJ. Water proton MR properties of human blood at 1.5 Tesla: magnetic susceptibility, T(1), T(2), T*(2), and non-Lorentzian signal behavior. Magn. Reson. Med. 2001; 45:533–42. [PubMed: 11283978]

Sukstanskii AL, Yablonskiy DA. Theory of FID NMR signal dephasing induced by mesoscopic magnetic field inhomogeneities in biological systems. J. Magn. Reson. 2001; 151:107–17. [PubMed: 11444944]

Sun X, Li XF, Russell J, Xing L, Urano M, Li GC, Humm JL, Ling CC. Changes in tumor hypoxia induced by mild temperature hyperthermia as assessed by dual-tracer immunohistochemistry. Radiother. Oncol. 2008; 88:269–76. [PubMed: 18538874]

van der Zee J. Heating the patient: a promising approach? Ann. Oncol. 2002; 13:1173–84. [PubMed: 12181239]

Waterman FM, Nerlinger RE, Moylan DJ 3rd, Leeper DB. Response of human tumor blood flow to local hyperthermia. Int. J. Radiat. Oncol. Biol. Phys. 1987; 13:75–82. [PubMed: 3804819]

Webb P, Spielman D, Macovski A. A fast spectroscopic imaging method using a blipped phase encode gradient. Magn. Reson. Med. 1989; 12:306–15. [PubMed: 2628681]

Yablonskiy DA, Haacke EM. Theory of NMR signal behavior in magnetically inhomogeneous tissues: the static dephasing regime. Magn. Reson. Med. 1994; 32:749–63. [PubMed: 7869897]

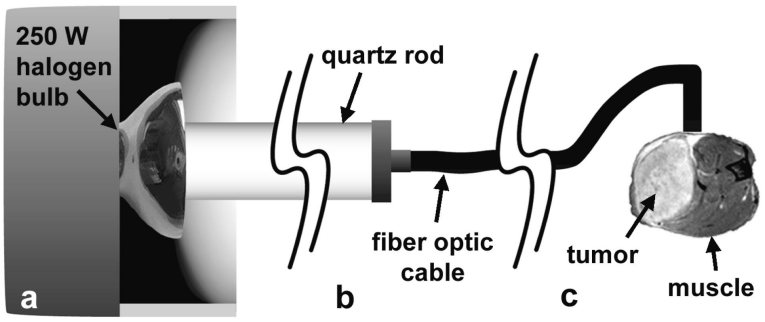

Figure 1.

Diagram of method used to induce hyperthermia in small localized region of tumor and normal muscle. (a) Light from a 250 W halogen blub is transmitted into a 1cm diameter quartz rod. (b) A 3 mm fiber optic cable was attached to the end of the quartz rod. (c) The fiber optic cable was manufactured with a 90° bend in the end. This was placed flush to the surface of the mouse leg such that the cross section of the cable face was bisected by the tumor/normal muscle interface. This design produced an increase in tissue temperature of ~6° C, as demonstrated in bench experiments.

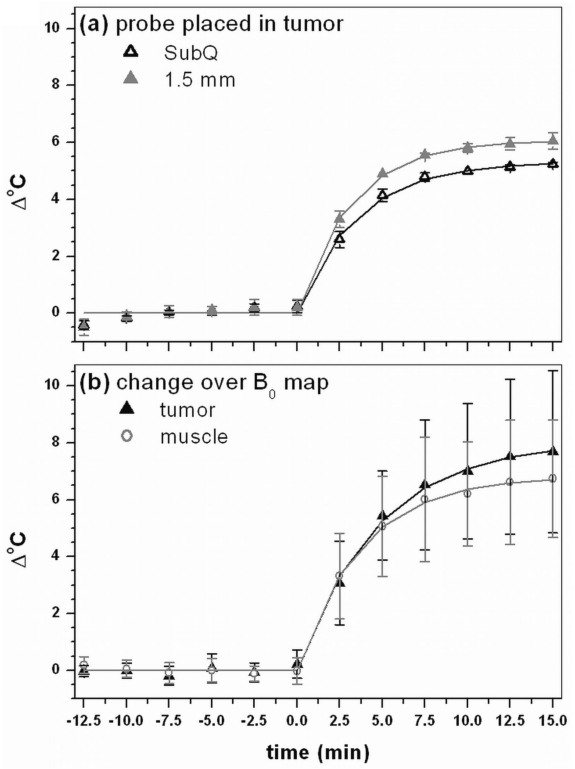

Figure 2.

(a) Average result of bench experiment with the temperature needle probe placed subcutaneously (SubQ) and 1.5 mm in the tumor tissue and (b) average change over all experiments in temperature in B_0 maps in tumor and muscle. Points indicate real data whereas solid lines indicate respective fits by equation (1) to data. All fits have a R^2 value greater than 0.995, indicating that equation (1) models the change in temperature using needle probes and the temperature dependent change in proton resonance frequency shifts very well.

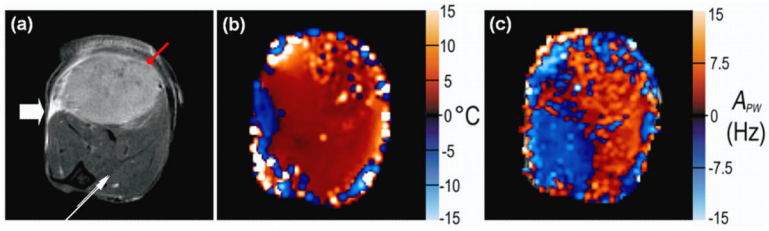

Figure 3.

The large white arrow in (a) indicates the position of the fiber optic light source as demonstrated in figure 1. (a) Spin echo image (displayed FOV = 12 mm × 12 mm) of typical tumor bearing hind leg for anatomic reference. The red arrow indicates tumor; the thin white arrow indicates boundary of two different muscle groups. In images (b - c), red scale indicates increasing positive changes and blue scale, negative changes, according to the label on the respective y-axis. (b) A_{Bo} map reflecting the maximum change in temperature in each voxel over the course of an experiment. Changes are typically 5°C. Very large changes are likely due to statistical fluctuations in B_0. The region of negative change next to the light source (as indicated by the white arrow) may be due to a large local change in magnetic susceptibility due to the proximity of the fiber optic cable. (c) A_{PW} values, reflecting maximum absolute changes in water peak width (in Hz).

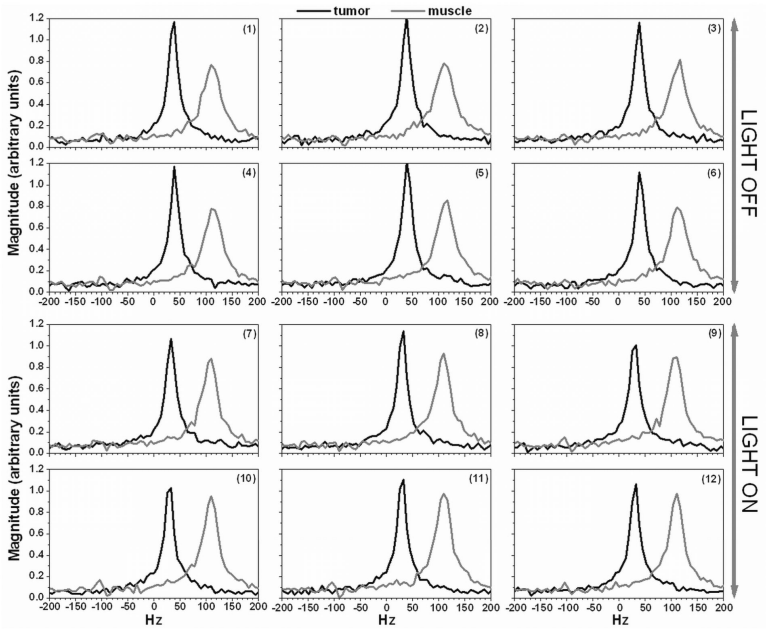

Figure 4.

Selected modulus spectra from a single voxel in tumor (black line) and in muscle (gray line) were plotted for HiSS data acquired with the light turned off (1- 6) and with the light on (7 - 12). The voxel in tumor and muscle were selected from the experiment showed in Figure 3.

Table 1

Calculated A_{pw} values (mean ± standard deviation) for tumor rim, tumor center, and muscle ROIs. Columns indicate the specific ROI being analyzed, the mean peak-width over the ROI during heating (post), the mean peak-width reported compared with baseline (pre) within the same ROI, and inter-ROI comparisons of reported mean peak-widths during heating.

a. Statistical analyses of positive A_{PW} values

ROI	MEAN ± STDEV (Hz)	*p* values			
		pre vs. post heating[a]	RIM [b]	CENTER[b]	MUSCLE [b]
RIM	9.96 ± 3.24	0.00005	-	0.43	0.08
CENTER	8.66 ± 3.98	0.0005	0.43	-	0.32
MUSCLE	7.01 ± 2.32	0.00006	0.08	0.32	-

b. Statistical analyses of negative A_{PW} values

ROI	MEAN ± STDEV (Hz)	*p* values			
		pre vs. post heating[a]	RIM [c]	CENTER[c]	MUSCLE [c]
RIM	−12.91 ± 4.53	0.00009	-	0.12	0.04
CENTER	−8.53 ± 3.53	0.0002	0.12	-	0.90
MUSCLE	−7.93 ± 1.44	0.00001	0.04	0.90	-

[a] Statistical significance was computed using a two-tailed, unpaired Student's t-test.

[b] Statistical significance was computed using a one-way analysis of variance (ANOVA) after normality was ensured using a Shapiro-Wilk test. Variance was found to be homogeneous by the Levene test; therefore a LSD *post hoc* test was applied to determine the *p*-value.

[c] Statistical significance was computed using a one-way analysis of variance (ANOVA) after normality was ensured using a Shapiro-Wilk test. Variance was found to be heterogeneous by the Levene test; therefore a Games-Howell *post hoc* test was applied to determine the *p*-value.